Microstructure of nonideal methanol binary liquid mixtures

I. Essafri and A. Ghoufi*

Institut de Physique de Rennes, UMR 6251 CNRS, Université de Rennes, 263 avenue Général Leclerc, 35042 Rennes, France

(Received 26 April 2019; published 19 June 2019)

The nonideality of binary mixtures is often related to the nature of the interactions between both liquids and of the heterogeneity at the nanoscale-named microstructure. When one of the liquids is a hydrogen bonds former and the second is aprotic, the progressive diluting of the hydrogen-bonding network leads to a clustering and nanophases. By considering two mixtures, toluene-methanol and cyclohexane-methanol, the nonideality and its connection with the structure at the nanoscale and the intermolecular interactions are numerically investigated. Contrary to the toluene that is fully miscible in methanol, cyclohexane presents a high range of immiscibility which makes it a relevant system to study the nucleation (local segregation) and its propagation. In both mixtures, the deviation from the ideal behavior is observed. In the case of the toluene-methanol mixture, the initial hydrogen-bonding network corresponding to a homogenous structure is locally broken due to the favorable toluene-methanol interactions leading to the spatial heterogeneity at the origin of the nonideality. In the range of miscibility of the cyclohexane-methanol mixtures, the formation of hydrophobic nanophases of larger size is observed due to the unfavorable interactions between both components leading to a self-organizing of cyclohexane molecules. The immiscibility of cyclohexane and methanol are then correlated to the formation of nanophases and their propagation, which are also at the origin of the spatial heterogeneity. In the pure methanol, we highlight the disconnection between the clustering and the heterogeneity. We shed light on the fact that the prepeak observed in the structure factor is independent of the degree of heterogeneity, but is connected to the presence of cyclic clusters.

DOI: 10.1103/PhysRevE.99.062607

I. INTRODUCTION

The hydrogen bond (HB), which is ubiquitous in self-assembly sciences including chemistry, biology, and physics, has been the subject of extensive investigation in the last 100 years [1–9]. Among the HB former liquids, many works have been devoted on water to connect the structure with the macroscopic properties [6,9] and more especially its physical anomalies [10]. Alcohols are a class of HB liquids such that the molecules form the HB from their hydroxyl group (OH), whereas their hydrophobic moiety provides them an amphiphilic character [11–30]. Regarding the primary alcohols, HB leads to a chainlike structure [31] which is less cohesive than the three-dimensional HB network of water, whereas the hydrophobic group is at the origin of the micellar structure (the molecular emulsion [32]). This amphiphilic behavior leads to the structural heterogeneities at the nanoscale although the homogeneity and the full mixing are at the macroscopic scale [21,32–34]. To microscopically characterize this heterogeneity and this microstructure, extensive experiments and simulations have been performed [21,32–34]. The most studied alcohols are probably methanol and ethanol given their intriguing aqueous microscopic structure [17,21,29,35,36] and their numerous applications [37–39]. The heterogeneity of these two alcohols was examined by progressively diluting the HB network by using water [23] and to a lesser extent from an aprotic or organic solvent [33,34]. Indeed, the amphiphilic nature of the alcohols thereby solubilizes a large range of organic solvents that increases the heterogeneity and involves a strong deviation of thermodynamic properties from the ideal mixture behavior [34]. From the hexane-ethanol binary liquid mixture, Perera *et al.* have recently shown that the hydrogen-bonded structure persisted and induced a subsequent local segregation of ethanol [33] which allowed them to investigate the differences between clustering and heterogeneity [33] and structurally evidenced the heterogeneity from a prepeak in the structure factor. The presence of clusters then will be disconnected to the prepeak and to the heterogeneity. More recently the concept of "simple disorder" was defined if the excess quantities are always smoothly varying functions of molar fraction, whereas the notion of "complex disorder" was connected to the local heterogeneity or molecular emulsion evidenced by sharp changes occurring in the excess quantities with change of sign [32]. Actually, these recent concepts could be used to microscopically understand the nonideality of binary mixtures.

This work aims then to numerically investigate the nonideality of the binary liquid mixtures and its connection with the structure at the nanoscale. To do so, binary liquid mixtures based on methanol were examined. Although one of the objectives of this work is the connection between the nonideality and the microstructure, it does not focus on the concept of nanoscale heterogeneity. Contrary to the aqueous mixtures, less work has been reported on the dilution of methanol from organic solvents liquids [30,33,34], and no structural studies have been attempted to microscopically characterize and

*aziz.ghoufi@univ-rennes1.fr

TABLE I. Number of molecules [n (MeOH), n (TOL), and n (CHX)], molar fraction (x_{MeOH}), and final simulated density ($\rho_{\mathrm{sim.}}$).

n (TOL-CHX)	n (MeOH)	x_{MeOH}	$\rho_{\mathrm{sim.}}^{\mathrm{TOL}}$ (kg m^{-3})	$\rho_{\mathrm{sim.}}^{\mathrm{CHX}}$ (kg m^{-3})
500	0	0	854.3	762.5
450	50	0.1	850.8	761.8
400	100	0.2	847.2	760.9
350	150	0.3	843.4	760.7
300	200	0.4	838.8	760.6
250	250	0.5	833.8	759.9
200	300	0.6	827.7	761.5
150	350	0.7	820.4	764.4
100	400	0.8	812.6	767.4
50	450	0.9	803.1	775.6
0	500	1	786.9	786.9

understand these mixtures. The emerging questioning deals with the molecular origin of the nonideality and its connection with the spatial heterogeneity. To address it, molecular dynamics simulations of two binary liquid mixtures, toluene-methanol and cyclohexane-methanol, were carried out. Contrary to the toluene, cyclohexane shows an immiscibility with methanol from a molar fraction (x_{MeOH}) of 0.13 to 0.79. This system is then suitable to microscopically study the progressive development of the immiscibility from $x_{\mathrm{MeOH}} = 0$ to 0.13 and the restoration of the miscibility from $x_{\mathrm{MeOH}} = 0.79$. The toluene was considered given its high hydrophobic character and the presence of a benzenic cycle that allows us to explore the role of the aromatic cycle in the miscibility of organic solvents in methanol.

The outline of this paper is as follows. In Sec. II we present the potentials and computational details. The results and discussions are provided in Sec. III. The main conclusions of this work are summarized in Sec. IV.

II. MODELS AND COMPUTATIONAL DETAILS

Methanol, toluene, and cyclohexane were modeled by the flexible nonpolarizable optimized potential for liquid simulations (OPLS) all atoms force field [40]. Indeed, it was recently shown that the OPLS models were quantitatively reproduced thermodynamical and interfacial properties [41,42]. The intermolecular interactions are composed of the repulsion-dispersion and the electrostatic contributions respectively modeled by the Lennard-Jones (LJ) and Coulombic potentials. The electrostatic interactions were truncated at 12 Å and calculated using the Ewald sum with a precision of 10^{-6}. Short-range interactions were modeled by using the Lennard-Jones potential using a cutoff of 12 Å. Here the interactions between unlike LJ sites of two molecules were determined by the Lorentz-Berthelot combining rule. The statistical errors for the calculated properties were estimated using the block averages method. Simulation boxes were cubic, and final dimensions along three axes ($\mathrm{L}_x = \mathrm{L}_y = \mathrm{L}_z$) are given in Table I. Periodic boundary conditions were applied in the three directions. MD simulations were performed in the NpT statistical ensemble such that N is the number of particles, T is the temperature, and p is the pressure. Molecular dynamics simulations were performed at $T = 300$ K and $p = 1$ bar using a time step of 0.001 ps to sample 10 ns (acquisition and equilibration phases). All MD simulations were carried out from the DL_POLY package [43] using a combination of the velocity-Verlet and the Nose-Hoover thermostat and barostat algorithms [44,45]. The initial configuration was built by a random distribution of methanol (MeOH), toluene (TOL), and cyclohexane (CHX) molecules. Eleven molar fractions in MeOH (x_{MeOH}) were investigated {0, 0.1, 0.2, 0.3, 0.4, 0.5, 0.6, 0.7, 0.8, 0.9, 1}. Number of molecules, molar fraction, and simulated density of mixtures are reported in Table I. As shown in Table I the total number of molecules is 500. To ensure our results and to avoid size effects, MD simulations with $N = 4000$ for five molar fractions ($x_{\mathrm{MeOH}} = 0$, 0.1, 0.5, 0.9, 1.0) were performed. Although the temperature and the enthalpy of simulations of 500 molecules converged, the mechanical equilibrium was ensured. To do so, the profile of the total pressure according to the z direction was computed. Calculation of pressure profiles were performed by using the nonexponential perturbation method [46] by considering the long-range corrections [47].

The total configurational energy U is defined by

$$U = U_{\mathrm{INTRA}} + U_{\mathrm{INTER}}, \tag{1}$$

where U_{INTRA}, U_{INTER} are the intramolecular and intermolecular energy contributions, respectively. U_{INTRA} is expressed as

$$U_{\mathrm{INTRA}} = U_{\mathrm{BONDS}} + U_{\mathrm{ANGLES}} + U_{\mathrm{DIHEDRALS}} + U_{\mathrm{NONBONDED}}, \tag{2}$$

such that

$$U_{\mathrm{BONDS}} = k_r(r - r_0)^2, \quad U_{\mathrm{ANGLES}} = k_\Theta(\Theta - \Theta_0)^2, \tag{3}$$

where r is the distance between two atoms, Θ is the valence angle between three atoms, k_r and k_Θ are the strengths of the bonds and valence angle, respectively, and r_0 and Θ_0 are the equilibrium distance and angle, respectively. The dihedral potential is expressed from a triple cosinus potential

$$U_{\mathrm{DIHEDRALS}} = A_0 + 0.5A_1[1 + \cos(\Phi)] + 0.5A_1[1 - \cos(2\Phi)] + 0.5A_3[1 + \cos(3\Phi)], \tag{4}$$

where A_1, A_2, and A_3 are the strengths of the dihedral angle. All parameters were described from the OPLS force field and can be found elsewhere [40]. The nonbonded terms are evaluated from the electrostatic and Lennard-Jones potential described below.

The intermolecular interactions are composed of repulsion-dispersion and electrostatic contributions that are represented by Lennard-Jones (LJ) and Coulombic (ELEC) potentials, respectively:

$$U_{\mathrm{INTER}} = U_{\mathrm{LJ}} + U_{\mathrm{ELEC}}, \tag{5}$$

$$U_{\mathrm{LJ}} = \sum_{i=1}^{N-1}\sum_{j>i}^{N}\sum_{a=1}^{N_i}\sum_{b=1}^{N_j} u_{\mathrm{LJ}}(r_{iajb}) = \sum_{i=1}^{N-1}\sum_{j>i}^{N}\sum_{a=1}^{N_i}\sum_{b=1}^{N_j} 4\epsilon_{ab}\left[\left(\frac{\sigma_{ab}}{r_{iajb}}\right)^{12} - \left(\frac{\sigma_{ab}}{r_{iajb}}\right)^{6}\right], \tag{6}$$

where r_{iajb} is the distance between force center a in molecule i and force center b in molecule j, ϵ_{ab} is the energy parameter of the interaction, and σ_{ab} is the LJ core diameter. N_i is the number of force centers in the molecule i. The LJ parameters for the interactions between unlike sites were calculated using the Lorentz-Berthelot combining rules

$$\epsilon_{ab} = (\epsilon_{aa}\epsilon_{bb})^{1/2}, \quad \sigma_{ab} = \tfrac{1}{2}(\sigma_{aa} + \sigma_{bb}). \tag{7}$$

The electrostatic interactions were calculated using the Ewald sum method from

$$\begin{aligned} U_{\mathrm{ELEC}} = {} & \frac{1}{2\epsilon_o V}\sum_{k\neq 0} Q(h)S(\mathbf{h})S(-\mathbf{h}) \\ & + \frac{1}{8\pi\epsilon_o}\sum_i\sum_a\sum_{j\neq i} q_{ia}\sum_b q_{jb}\,\mathrm{erfc}\,(\alpha r_{iajb})/r_{iajb} \\ & - \frac{\alpha}{4\pi^{3/2}\epsilon_o}\sum_i\sum_a q_{ia}^2 \\ & - \frac{1}{8\pi\epsilon_o}\sum_i\sum_a\sum_{b\neq a}\frac{q_{ia}q_{ib}}{r_{iaib}}\mathrm{erf}(\alpha r_{iaib}), \end{aligned} \tag{8}$$

where $\mathrm{erfc}(x)$ is the complementary error function and $\mathrm{erf}(x)$ is the error function. α is chosen so that interaction pairs only in the central cell need to be considered in evaluating the second term in Eq. (8). The functions $S(\mathbf{h})$ and $Q(h)$ are defined using Eqs. (9) and (10), respectively:

$$S(\mathbf{h}) = \sum_i\sum_a q_{ia}\exp(i\mathbf{h}\cdot\mathbf{r_{ia}}), \tag{9}$$

$$Q(h) = \frac{1}{h^2}\exp\left(-\frac{h^2}{4\alpha^2}\right), \tag{10}$$

where the reciprocal lattice vector $\mathbf{h}$ is defined as $\mathbf{h} = 2\pi(l/L_x\mathbf{u}, m/L_y\mathbf{v}, n/L_z\mathbf{w})$, where $\mathbf{u}, \mathbf{v}, \mathbf{w}$ are the reciprocal space basis vectors and l, m, n take values of 0, ±1, ±2, $\ldots, \pm\infty$. The reciprocal space sum is truncated at an ellipsoidal boundary at the vector $|\mathbf{h}^{\max}|$. The convergence factor α is calculated from $\frac{2\pi}{L_x}$. The maximum reciprocal lattice vectors parallel to the surface $|\mathbf{h}_x^{\max}|$ and $\mathbf{h}_y^{\max}|$ were fixed to 8 and $|\mathbf{h}_z^{\max}|$ to 48. The increase in $|\mathbf{h}_z^{\max}|$ is required to accurately account for the long-range electrostatic interactions in the direction normal to the interface due to a larger dimension box in this direction.

III. RESULTS AND DISCUSSION

A. Simulation validation

We report in Fig. 1(a) the density of the liquid phase as a function of x_{MeOH} for both mixtures. In two cases the so-calculated densities are found in fair agreement with the experiments [48,49] that validate the models used to describe MeOH, CHX, and TOL molecules and their combining interactions. Experimentally, the CHX-MeOH mixture is well known to demix between $x_{\mathrm{MeOH}} = 0.2$ and $x_{\mathrm{MeOH}} = 0.8$. This tendency to segregate is highlighted in Fig. 1(c) where snapshots of CHX-MeOH at $x_{\mathrm{MeOH}} = 0.1$, 0.5, and 0.9 are reported. As shown in Fig. 1(c) the phase separation is well recovered at $x_{\mathrm{MeOH}} = 0.5$, whereas at $x_{\mathrm{MeOH}} = 0.1$ and 0.9 the systems are miscible. This result is in good agreement with the experimental immiscible region [Fig. 1(a)] that allows us to be confident in the OPLS force field used. Moreover, as evidenced in Fig. 1(a) the so-calculated densities with higher systems (4000 molecules) are found in good concordance with simulations of 500 molecules that involve a small impact of size effects, which bears out our computational procedure. The mechanical equilibrium of MD simulations of 500 molecules was checked by calculating the profile of the total pressure according to the z direction. Given the isotropy of our system, the profiles according to the x, y, and z directions were found similar.

We report in Fig. 2(a) the profile of the total microscopic pressure along the z direction for the CHX-MeOH for three methanol molar fractions: $x_{\mathrm{MeOH}} = 0.1$, 0.5, and 0.9. Let us mention that the so-calculated microscopic pressure was averaged on all configurations. Macroscopic pressure fluctuations that are on an order of hundreds of bar are typical. From the local pressure calculation, a maximum of fluctuations around 10 Mpa was found for $x_{\mathrm{MeOH}} = 0.1$ and around 3–5 Mpa for other concentrations. Indeed, the pressure is a macroscopic property and can be measured properly only as a time average. As shown in Fig. 2(a) the pressure is constant along the z direction, highlighting that the mechanical equilibrium is well reached. As exhibited in Fig. 2(a) the pressure oscillations are the same order of magnitude as that for the calculated pressure for the water reference system and that for the profile pressures reported in the literature [50]. The pressure profile was also calculated for $x_{\mathrm{MeOH}} = 0.5$ for a system of 4000 molecules. As highlighted in Fig. 2(a) the pressure profile is in good concordance with the calculated pressure for the system of 500 molecules, which suggests that the studied systems of 500 molecules are physically relevant to capture the microscopic insights into both binary mixtures. Interestingly, Fig. 2(a) shows that at $x_{\mathrm{MeOH}} = 0.5$, i.e., for the demixing system, the pressure profile is constant, highlighting the mechanical pressure [50–53] through the interface between methanol and cyclohexane.

B. Nonideality and structural heterogeneity

As exhibited in Fig. 1(a), the density of the TOL-MeOH mixture presents a monotonic evolution as a function of x_{MeOH}, whereas the CHX-MeOH mixture shows a minimum around $x_{\mathrm{MeOH}} = 0.5$. Additionally, both mixtures present a deviation of the same order of magnitude in relation to the ideal density calculated from $\rho = x_{\mathrm{MeOH}}\rho_{\mathrm{MeOH}} + (1 - x_{\mathrm{MeOH}})\rho_{\mathrm{CHX/TOL}}$. Very interestingly, the CHX-MeOH mixture also presents a nonideal behavior in the miscible regions. To quantify this nonideality, we report in Fig. 1(b) the excess density of the mixtures as a function of x_{MeOH}. The excess density was evaluated as the difference between the simulated and the ideal densities. As exhibited in Fig. 1(b) the CHX-MeOH and the TOL-MeOH mixtures display a negative and a positive excess density, respectively. Moreover, Fig. 1(b) shows that both TOL-MeOH and CHX-MeOH mixtures present a change in monotony of the excess density. Furthermore, in the two miscible and immiscible zones the nonideality of the CHX-MeOH mixture (absolute value of the excess density) is higher than the TOL-MeOH one. These behaviors could be imputed

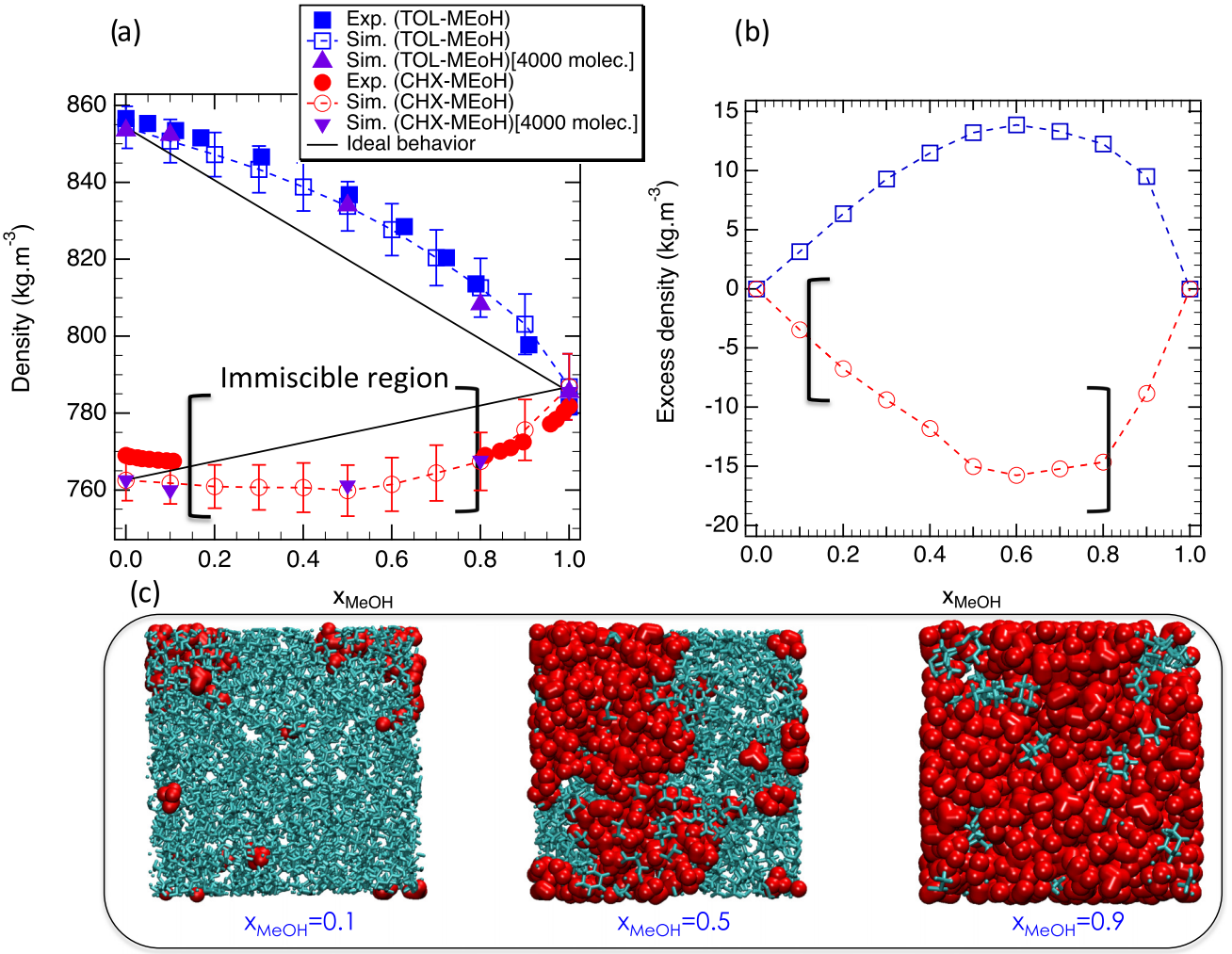

FIG. 1. Simulated and experimental density (a) and the excess density (b) of the CHX-MeOH and TOL-MeOH mixtures as a function of x_{MeOH} at 300 K and 1 bar. The uncertainties about the density are too small to be represented. (c) Snapshots of binary mixture at $x_{\mathrm{MeOH}} = 0.1$, 0.5, and 0.9 such that methanol is represented in red spacefill, and CHX is represented in stick cyan.

to a change in the structural topology [18,29] leading to a structural heterogeneity or a difference in the interactions between both components of the binary liquid mixture [54]. Actually, contrary to the miscible zone, in the immiscible region of the CHX-MeOH mixture the difference is due to the phase separation.

Interestingly, as illustrated in Fig. 3, it seems that the immiscibility at a low methanol concentration is due to the formation of the methanol pocket assimilated to a nucleation process leading to the formation of nanophases rich in methanol molecules such that the OH groups are hidden from the organic solvent given the lack of favorable interactions. The progressive formation of nanophases could then generate a structural heterogeneity. At high concentration in methanol ($x_{\mathrm{MeOH}} = 0.8$) the miscibility is recovered due to the percolating of the methanol nanophases. Actually, in the miscible region, the progressive formation of these nanophases increases the heterogeneity and could explain the nonideality of the CHX-MeOH mixture.

To quantify this spatial heterogeneity, the heterogeneity order parameter (HOP) [55,56] was calculated from $\mathrm{HOP} = \frac{1}{N_s}\sum_{i=1}^{N_s}\sum_{i=1}^{N_s}\exp\left(-\frac{r_{ij}^2}{2\sigma^2}\right)$ such that N_s is the total number of sites in the system that represents the centers of mass of molecules, r_{ij} is the distance between sites i and j, and $\sigma = \frac{L}{N_s^{\frac{1}{3}}}$, L is the length of the cubic simulation box. The HOP value increases with the expansion of the spatial heterogeneity because a tighter packing of sites results in a smaller r_{ij}, which leads to a larger HOP. Calculations were performed for both binary liquid mixtures. According to the study of Wang *et al.*, the HOP of ideal particles homogeneously distributed is lower than 15.74, and a heterogeneous system exhibits a HOP greater than 15.74 [55]. We report in Fig. 2(b) the HOP value of each component as a function of the molar fraction in MeOH. First, in the pure MeOH liquid, the HOP is smaller than 15.74 highlighting the absence of spatial heterogeneity. Furthermore, as shown in Fig. 2(b), the addition of TOL or CHX molecules in the MeOH liquid generates spatial heterogeneity. In the miscible zone of the CHX-MeOH mixture, the HOP of methanol is higher than that in the TOL-MeOH mixture. As underlined in Fig. 3, that is the result of the formation of nanophases of methanol

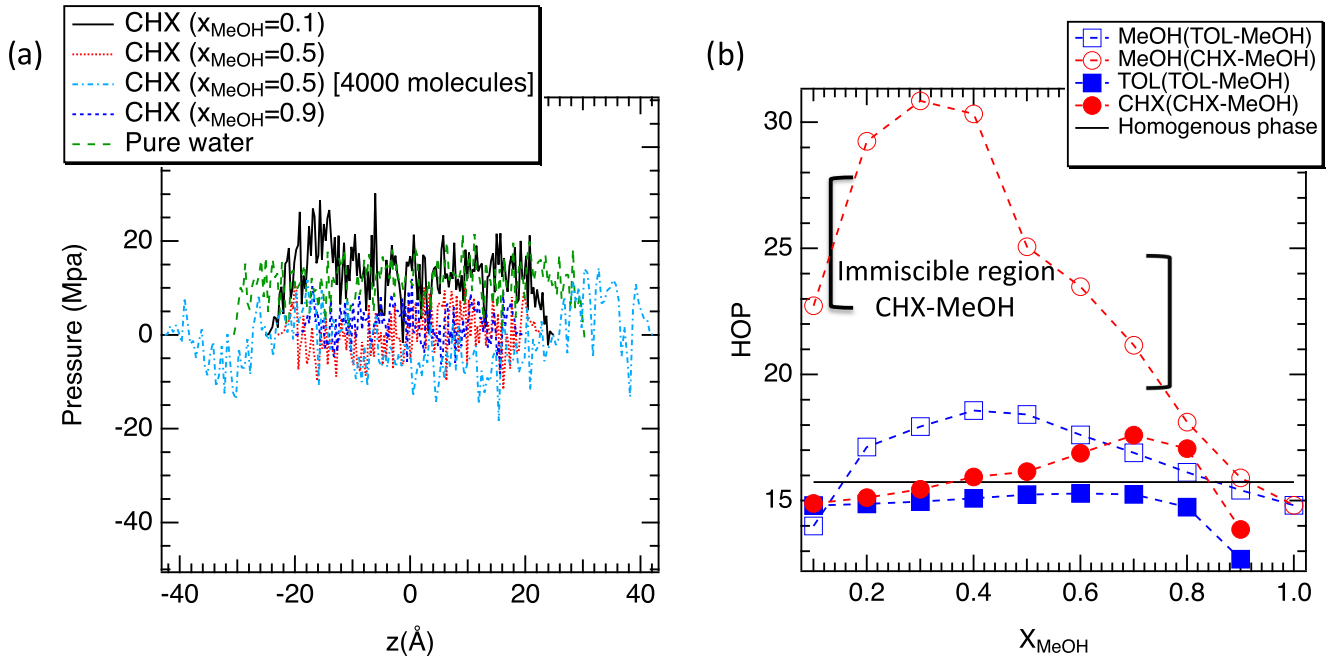

FIG. 2. (a) Profiles of the total pressure along the z direction for three methanol concentrations of the CHX-MeOH mixtures and for water at 1 bar and 300 K. (b) HOP as a function of the molar fraction in MeOH for both CHX-MeOH and TOL-MeOH mixtures.

preceding the phase separation. The nonideality behavior of the CHX-MeOH mixture therefore can be imputed to the strong heterogeneity in the miscible phase. That is probably the result of a lack of favorable interactions between CHX and MeOH. Contrary to the CHX-MeOH mixture, MeOH in TOL-MeOH shows a smaller HOP. Indeed, at $x_{MeOH} = 0.1$ HOP of MeOH is around 14 and 23 in TOL-MeOH and CHX-MeOH mixtures, respectively. In the case of the TOL-MeOH mixture, the HOP increases as a function of x_{MeOH} and is greater than 15.74 highlighting a microstructure. Let us mention that the microstructure is assimilated to the presence of the heterogeneities, and both terms will be subsequently used interchangeably. Whereas the spatial heterogeneity in the CHX-MeOH mixtures is the result of the local segregation and its propagation to strive for a total demixing, the molecular origin of the microstructure in the TOL-MeOH mixtures is then yet to be determined. Interestingly, Fig. 2(b) highlights that the HOP of CHX and TOL (close to 15) is lower than

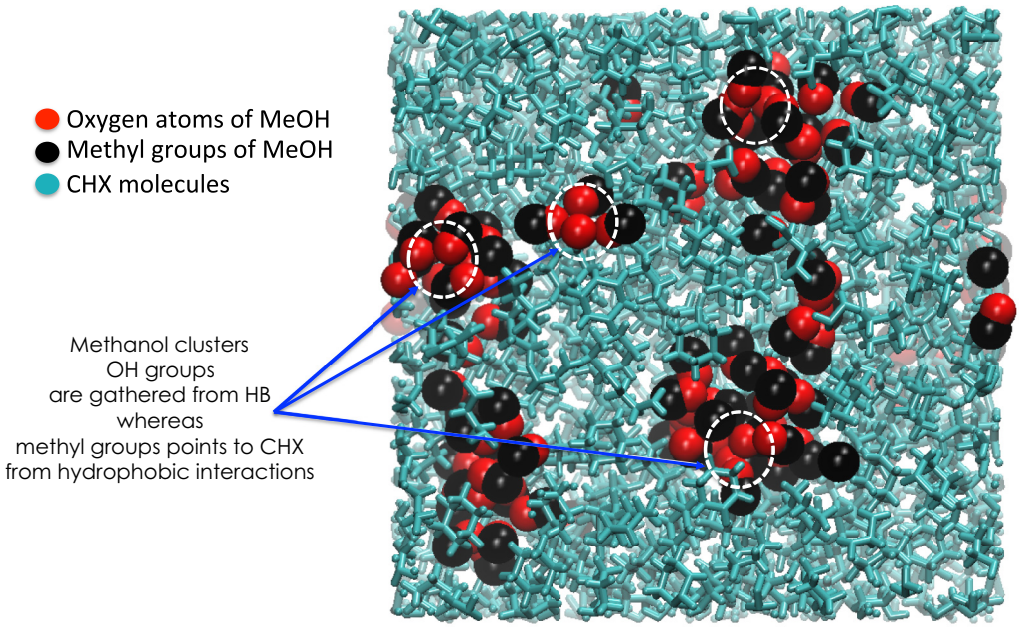

FIG. 3. Snapshot of the CHX-MeOH mixture at $x_{MeOH} = 0.2$ such that oxygen atoms and the methyl groups of the methanol are represented in red and black spacefill, respectively. CHX is represented in stick cyan.

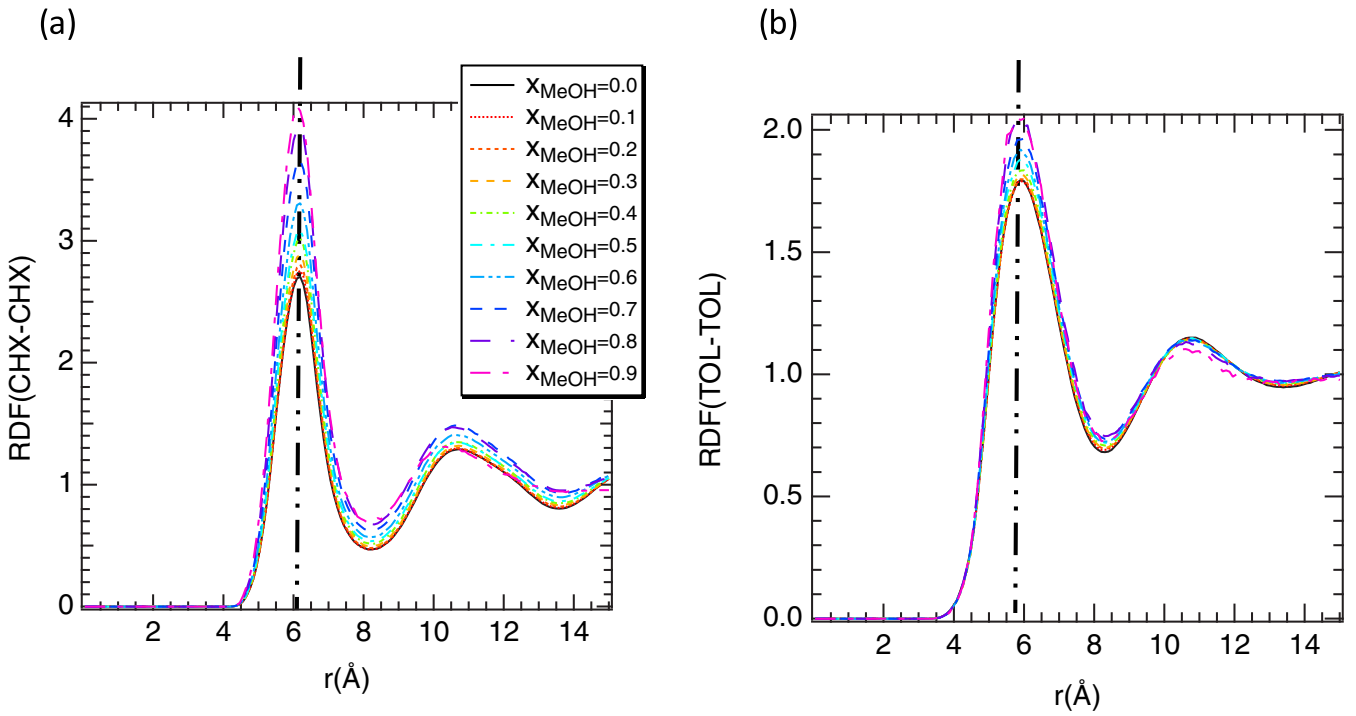

FIG. 4. Radial distribution functions between centers of mass of the aprotic component for both CHX-MeOH (a) and (b) TOL-MeOH mixtures. The vertical dashed line represents the position of the first peak.

the HOP of MeOH, which suggests a more homogenous distribution of the aprotic component in the mixtures.

C. Molecular interactions

To unveil the driving force ruling this miscibility and this nonideal behavior of TOL we report in Fig. 4 the radial distribution functions (RDFs) between the centers of mass of the aprotic component (TOL-TOL and CHX-CHX). The RDF was calculated from $\mathrm{RDF}(i-j) = \langle H(r_{ij})\rangle\langle V\rangle/4\pi r_{ij}^2\Delta r_{ij}N_iN_j$ such that $H(r_{ij})$ is the number of i-j pairwise interactions located at r_{ij}, V is the volume, r_{ij} the distance between i and j particles, N_i and N_j the number of i and j particles respectively, and $\langle\cdot\rangle$ the statistical

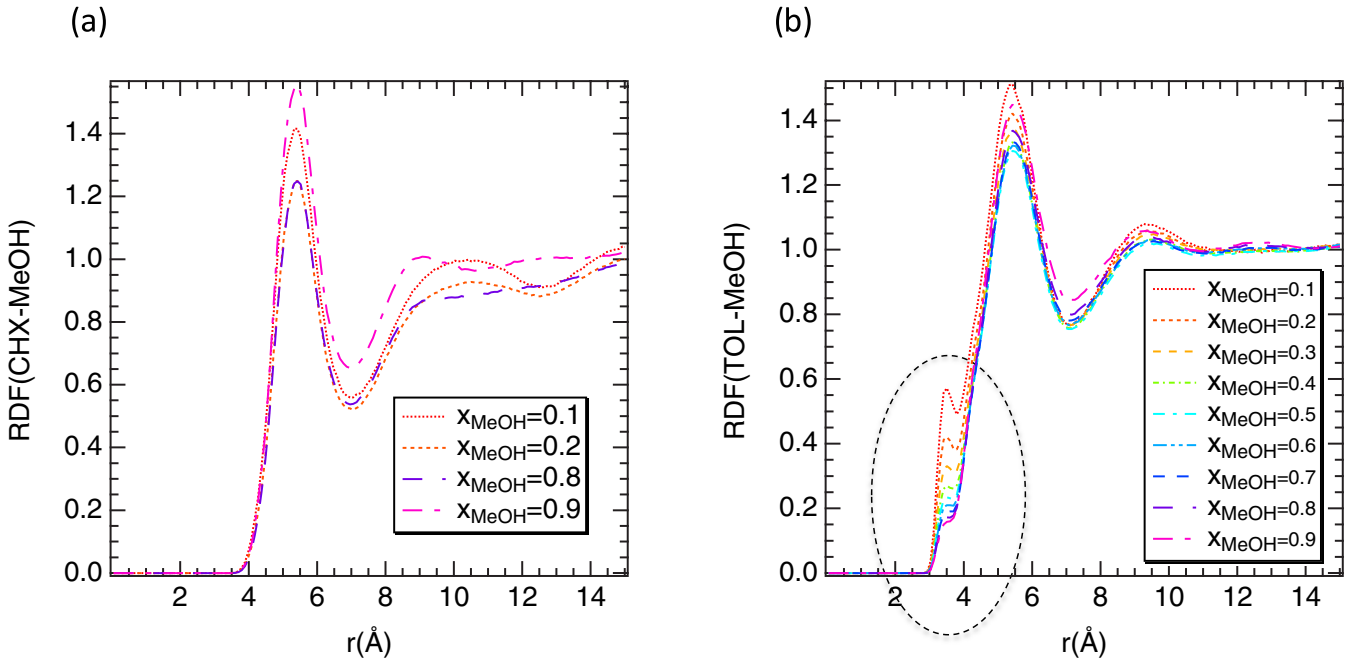

FIG. 5. Radial distribution functions between centers of mass of aprotic component and methanol for both CHX-MeOH (a) and TOL-MeOH (b) mixtures in the miscible regions. The dashed circles highlights the peaks located around 3.5 Å.

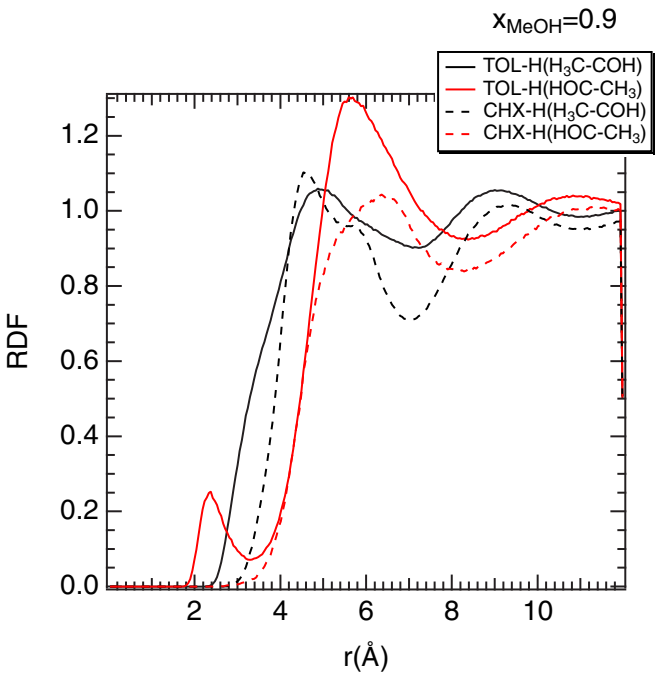

FIG. 6. Radial distribution functions between the center of mass of the aprotic molecules and the hydrogen atoms of OH (HOC) and CH_3 (H_3C) groups of methanol for $x_{MeOH} = 0.9$.

average. As shown in Figs. 4(a) and 4(b) the first peak of RDF(CHX-CHX) and RDF(TOL-TOL) is, respectively, located at 6.1 Å and 5.9 Å, highlighting a stronger interaction between toluene molecules due to the interactions between the aromatic cycles (this point will be discussed later). Furthermore, as highlighted in Figs. 4(a) and 4(b) the amplitudes of the first and second peak in both mixtures increase for the concentrated methanol solutions, whereas the shape and the position of the peaks are less sensitive to the dilution. The increase of the peaks' intensity then involves a higher local concentration in TOL (or CHX), which means that the probability of finding a TOL (or CHX) molecule at a distance r from another molecule does not scale with the decrease of the TOL (or CHX) number density, but it actually decays to a smaller extent [17]. That is an obvious evidence of the microstructure and the partial mixing at the molecular scale [17]. In case of the CHX-MeOH mixture, this effect is higher because the increase in RDF intensity as a function of the decrease in x_{MeOH} is more pronounced, suggesting an increase in the spatial heterogeneity in line with the HOP calculations and the miscible regions. Interestingly, this increase in intensity is similar to that observed in nanoconfined media where the excluded volume involves an increase in the interfacial concentration of confined fluids [15,57–59] and bears out the presence of nanophases.

Let us mention that the similar behavior is also observed with the second peak but to a lesser extent. To investigate the interactions between MeOH and TOL (CHX), the radial distribution functions between the centers of mass were calculated in the miscible regions and reported in Fig. 5. As shown in Fig. 5(a) the location of the first peak is found around 6 Å, highlighting a hydrophobic character of the CHX-MeOH interactions and the absence of specific interactions. Additionally, as stated earlier the increase in intensity with the decrease in x_{MeOH} is the result of the heterogeneity and the formation of nanophases. Interestingly, Fig. 5(a) reveals a second peak at low concentrations ($x_{MeOH} = 0.1$ and 0.2) synonymous with favorable interactions, which disappears between $x_{MeOH} = 0.2$ and $x_{MeOH} = 0.8$ to reappear at $x_{MeOH} = 0.9$, that is in fair agreement with the gap of miscibility observed in Fig. 1. Regarding the TOL-MeOH mixture, Fig. 5(b) displays a first peak around 3.5 Å underlining a strong interaction between

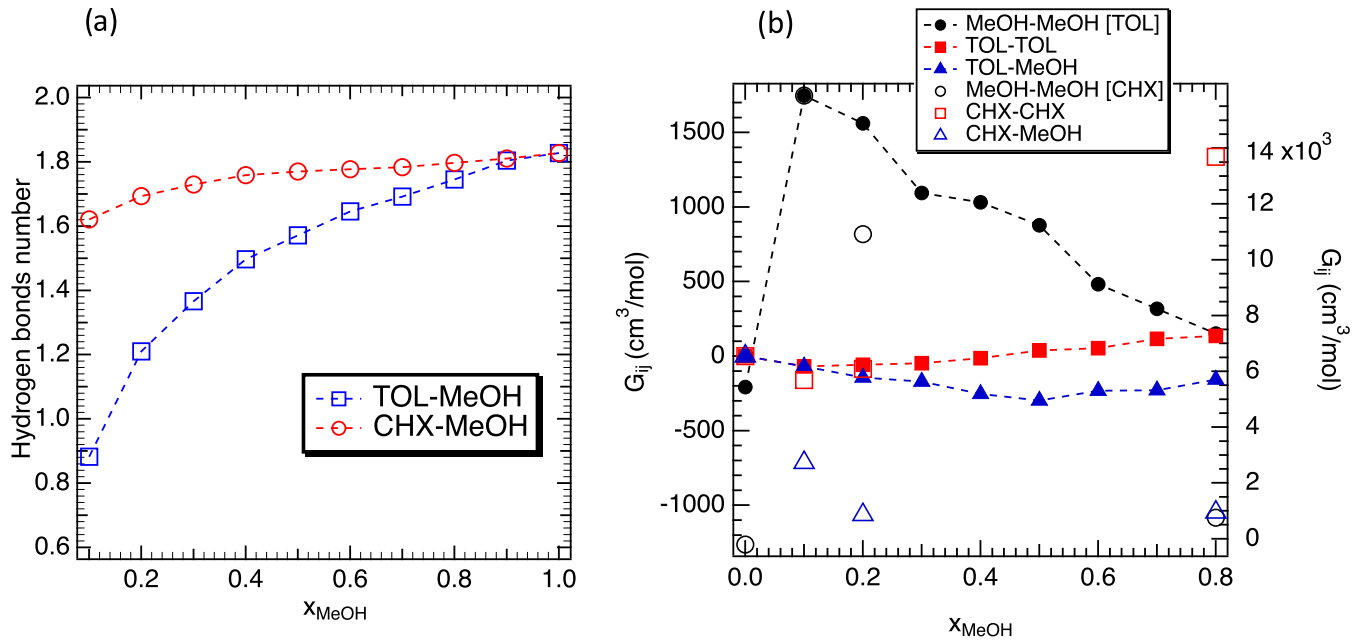

FIG. 7. (a) nHB per methanol molecule as a function of the methanol concentration. (b) KBIs as a function of the methanol concentration for both TOL-MeOH and CHX-MeOH mixtures. In panel (b) the right axis corresponds to the MeOH-MeOH KBI for the CHX-MeOH mixture.

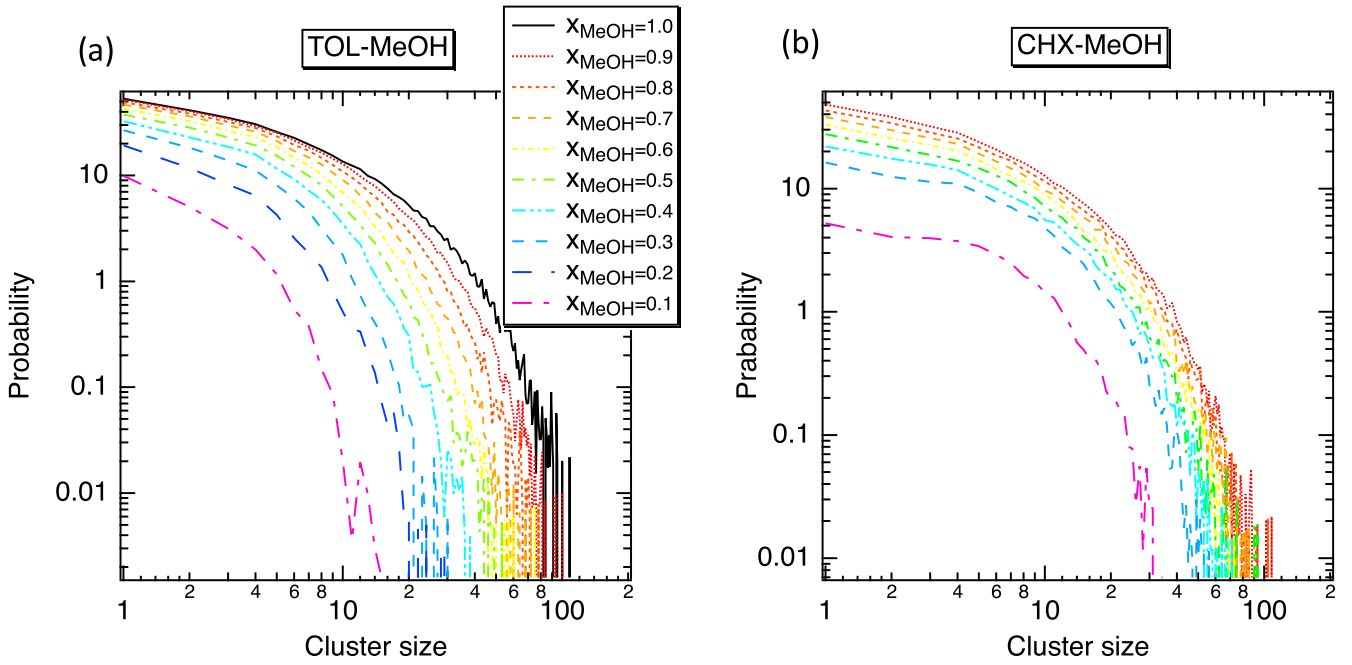

FIG. 8. Cluster size probability as a function of the MeOH concentration in logarithmic scale in both TOL-MeOH (a) and CHX-MeOH (b).

toluene and methanol molecules. This result sheds light on a preferential interaction between methanol and toluene.

To identify it, we report in Fig. 6 the RDF between the centers of mass of the aprotic component and hydrogen atoms of the hydroxyl and methyl groups of methanol. Let us mention that the center of mass of both TOL and CHX molecules is close to the center of the cycle. Figure 6 highlights a strong interaction between OH groups and toluene molecules because a distance of 2.5 Å was found that is the same order of magnitude as that of a HB. This result suggests then a HB-like interaction probably induced by the aromatic cycles. Actually, this strong interaction is probably at the origin of the toluene miscibility in methanol and the positive excess density [54]. In the CHX-MeOH mixtures the CHX molecules self-organize to form hydrophobic nanophases.

To characterize the microstructure in both mixtures the number of HBs per methanol molecule (nHB) was calculated. HBs were evaluated by considering the geometric criterion developed by Luzar and Chandler [2] such that the distance between a hydrogen atom of one MeOH molecule and the oxygen atom of another one has to be smaller than 2.5 Å whereas the distance between two oxygen atoms of two MeOH molecules has to be smaller than 3.5 Å. We report in Fig. 7(a) nHB as a function of x_{MeOH} for both mixtures. Concerning the CHX-MeOH mixture, Fig. 7(a) shows a slight monotonic decrease in nHB because we move from 1.8 to 1.6, whereas a strong diminution is observed in case of the TOL-MeOH mixture, which loses one HB by moving from 1.8 to 0.8. Concerning the CHX-MeOH mixtures, the progressive formation of nanophases allows us to conserve the nHB constant during the diluting. Indeed, the MeOH molecules are gathered in clusters, such that the OH groups are hidden from the CHX. In case of the TOL-MeOH mixture, the hydrogen-bonding network is broken in favor of the interactions between

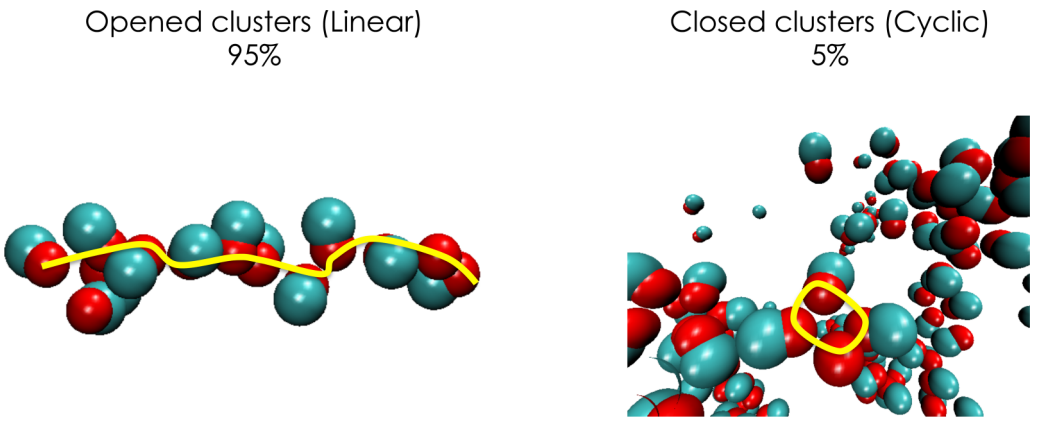

FIG. 9. Illustrations of opened and closed clusters highlighted with the yellow solid lines. Red and cyan correspond to the oxygen atoms and methyl groups, respectively.

TOL and MeOH molecules. That could suggest an increase in the dispersed MeOH molecules. This organization could be in line with an increase of small MeOH clusters (monomers and dimers) contrary to the CHX mixture where larger clusters could be favored. The increase in number of monomers and dimers in the TOL-MeOH mixture will be in accordance with the decrease of nHB.

To be thorough, the analysis of the molecular interactions through Kirkwood-Buff integrals (KBIs) was carried out for both TOL-MeOH and CHX-MeOH mixtures. KBIs were calculated from corrected RDF calculations by considering the recent development purposed by Krüger and coworkers improving the KBIs' convergence [60,61]. Details of calculations can be found in Refs. [60,61]. The KBIs at the thermodynamic limit ($V \to \infty$) between two types of molecules i and j such that V represents the volume of the system is notated G_{ij}^{∞} and is calculated from the following relation:

$$G_{ij}^{\infty} = \int_0^R 4\pi \left[g_{ij}^c(r) - 1\right] \times \left(1 - \frac{23}{8}x^3 + \frac{3}{4}x^4 + \frac{9}{8}x^5\right) r^2 dr, \quad \text{such that } x = \frac{r}{R}, \tag{11}$$

where $g_{ij}^c(r)$ is the corrected radial distribution function [61]. We report in Fig. 7(b) G_{ij} for all ij contributions in both TOL-MeOH and CHX-MeOH mixtures. In the case of the TOL-MeOH mixture, the predicted KBIs values are found in fair agreement with the experiment [34], suggesting that the calculation developed by Krüger and coworkers is well suitable to explore the binary liquid mixtures with microstructure. As exhibited in Fig. 7(b) G_{ij} of MeOH-MeOH interactions is positive in both mixtures, indicating the favorable interactions. Furthermore a maximum is found at very low concentration in methanol ($x_{\text{MeOH}} = 0.2$) could corresponds to the formation of the methanol cluster. The decrease in G_{ij} from $x_{\text{MeOH}} = 0.2$ could be probably due to the percolation of the hydrogen-bonding network where the interactions between methanol molecules are averaged. Cluster analysis and percolation of the hydrogen-bonding network will be analyzed in the following section. Interestingly, Fig. 7(b) shows that the KBIs of MeOH-MeOH interactions in the CHX mixtures are higher than in TOL ones. That is the result of unfavorable interactions between CHX and MeOH molecules increasing the formation of methanol clusters and then their interactions. TOL-TOL and CHX-CHX KBIs are strongly smaller than MeOH-MeOH ones, which suggests weaker interactions given their hydrophobicity and their weak polarity. Let us mention that the crossed interactions are negative is evidence of the unfavorable interactions in comparison with self-interactions. Eventually, we observe that $G_{\text{CHX-MeOH}}$ are more negative than $G_{\text{TOL-MeOH}}$, which is in line with the observed immiscibility between CHX and MeOH.

D. Cluster analysis

We report in Fig. 8 the cluster size distribution of MeOH for both TOL-MeOH and CHX-MeOH mixtures. In both cases and in all range of concentrations the system does not percolate to form only one interconnected network [8] even if

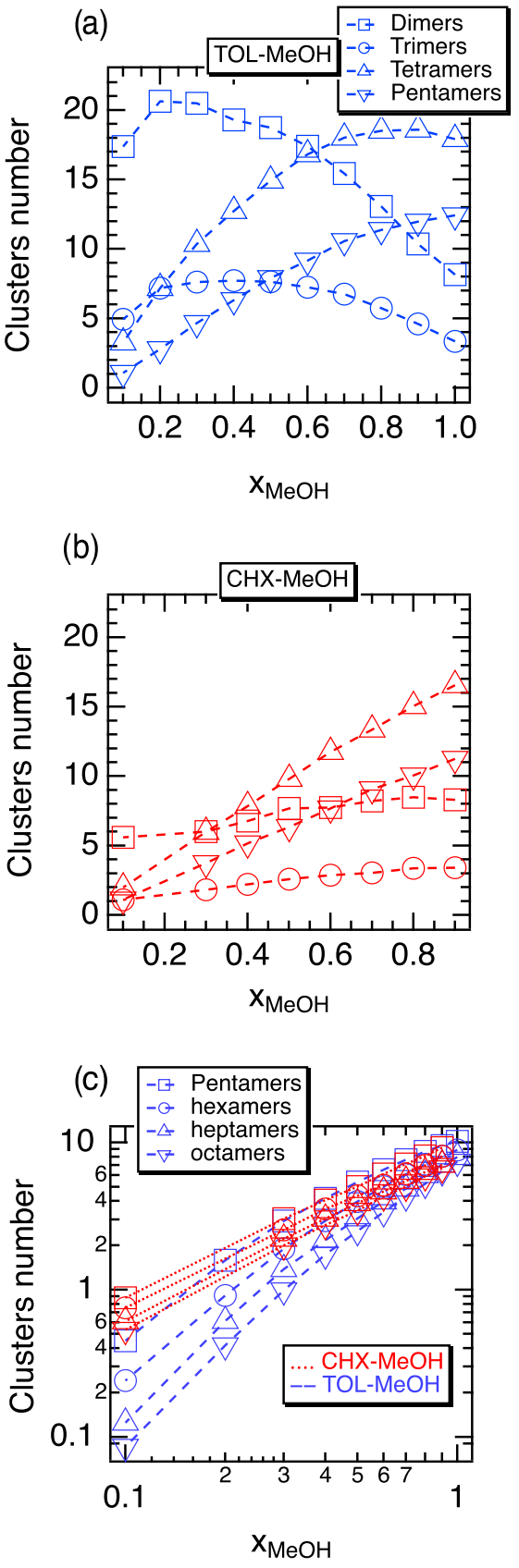

FIG. 10. Cluster number as a function of the MeOH concentration for the dimers, trimers, tetramers, and pentamers in both TOL-MeOH (a) and CHX-MeOH (b). (c) Number of higher clusters for both TOL-MeOH and CHX-MeOH mixtures.

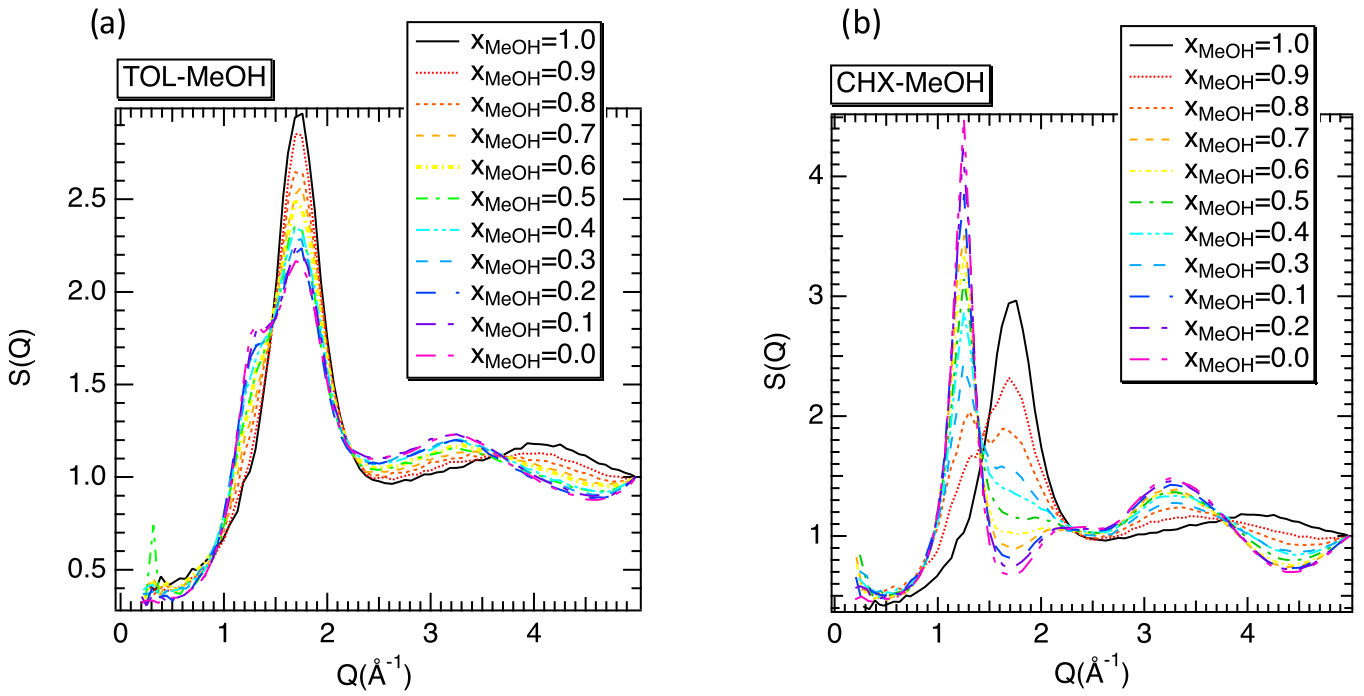

FIG. 11. Total structure factor of the TOL-MeOH (a) and CHX-MeOH (b) mixtures as a function of methanol concentration.

the cluster size increases as a function of the MeOH concentration. That could suggest the formation of methanol clusters of different sizes leading to a microstructure. From $x_{MeOH} = 0.2$ to $x_{MeOH} = 0.8$ (i.e., in the immiscible region) a broader size distribution of clusters is observed in the CHX-MeOH mixtures involving a wider size range of clusters. Additionally, the size cluster distribution in TOL-MeOH mixture is decreasing faster than in the CHX-MeOH mixture. Actually, these two facts suggest an increase in the heterogeneity and the development of the segregation process. Moreover, a faster decrease of the size distribution as the MeOH concentration increases is observed in the TOL-MeOH mixture. As shown in Fig. 8 small clusters are favored in case of the TOL-MeOH mixture, highlighting a better dispersion of toluene molecules in the mixture that is in good accordance with the miscibility of toluene in MeOH. The rates of the linear (opened structure) and cyclic (closed structure) clusters were also evaluated. In both cases and in the full range of MeOH concentration, a high proportion of linear structures (>96%) was found. We report in Fig. 9 examples of opened and closed structures.

We report in Figs. 10(a) and 10(b) the clusters number from dimers to pentamers in both mixtures. Strikingly, at low concentrations the number of short clusters is four times higher in the TOL-MeOH mixtures compared with the CHX-MeOH mixtures. Additionally, Fig. 10 exhibits a rapid decrease of the number of dimers and trimers as a function of the methanol concentration whereas the number of largerclusters increases. This result highlights the presence of clusters of different sizes leading to a spatial heterogeneity and then the microstructure. On the other hand, in the CHX-MeOH mixtures, a slight increase of the number of dimers and trimers is highlighted, while a linear progression is observed for the number of tetramers and pentamers. This result exhibits the presence of nanodomains of different sizes related to a spatial heterogeneity in both mixtures ruled by different types of interactions. The linear increase in clusters number into the CHX-MeOH mixtures could be connected to the growth of the MeOH domains during the phase separation. Figure 10(c) depicts a greater number of higher clusters in the CHX-MeOH mixture, thus bearing out the growth of the MeOH phase. Therefore, the difference in miscibility and in heterogeneity could be understood in terms of cluster size and distribution.

E. Clusters versus heterogeneity

Recently, Perera *et al.* have suggested that the structural signature of the heterogeneity and then the microstructure of ethanol mixture were related to the observation of a prepeak in the structure factor around 0.8 Å^{-1} [33]. More recently, Hureau *et al.*, by studying *tert*-butanol, have established that the prepeak was rather the structural signature of the presence of the closed clusters [26,58]. The structure factor [S(Q) such that Q is the momentum transfer vector] was calculated in both mixtures to structurally highlight the microstructure. All details of the structure factor calculation can be found elsewhere [26]. Let us mention that the value of S(Q = 0) was not evaluated because at Q = 0 Å^{-1} the system is poorly sampled, which explains that S(Q) begins from Q = 0.19 Å^{-1}. Indeed, Q = 0 Å^{-1} corresponds to the very high distance in the real space that was slightly sampled in our finite MD simulations. We report in Figs. 11(a) and 11(b) the total structure factor of both TOL-MeOH and CHX-MeOH mixtures, respectively, as a function of the methanol concentration. The total structure factor corresponds to the case where all atoms were considered. In both mixtures, Fig. 11 exhibits the absence of a prepeak that is contradicts the fact that the prepeak could be the structural signature of the heterogeneity. However, this

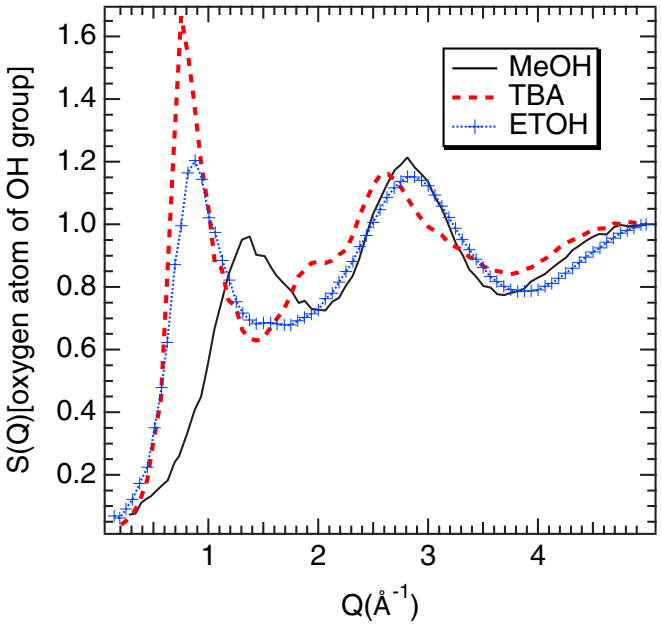

FIG. 12. Partial structure factor of the oxygen atom of the OH group of methanol, ethanol, and *tert*-butanol liquids at 1 bar and 300 K.

result is in line with the fact that the prepeak is connected to the closed clusters (5% of cyclic clusters in both mixtures). Indeed, physically, the prepeak at low Q can be assigned to the mesoscale spatial correlations between the hydrophilic parts surrounded by a hydrophobic shell. This situation occurs from molecules with a large hydrophobic moiety such as *tert*-butanol [26] (TBA) or ethanol [8] (ETOH). By using the previous data obtained from molecular simulation of TBA [26] and ETOH [8], we report in Fig. 12 the partial structure factor of the hydroxide groups. A partial structure factor allowed us to highlight the prepeak of the total structure factor that becomes the main one [26]. Details of the calculation of thee partial structure factor can be found in Ref. [26]. As shown in Fig. 12, TBA and ETOH present a first peak at 0.8 Å^{-1}, contrary to MeOH, which presents a first peak located at 1.4 Å^{-1}. The decrease of amplitude is the result of the decrease in the number of cyclic clusters. Indeed, in the TBA and ETOH liquids 95% and 15% of cyclic clusters were calculated, respectively, whereas in the pure methanol liquid, the rate of cyclic clusters is close to 5%. The shift from 0.8 to 1.4 Å^{-1} sheds light on range of mesoscopic correlations and on the size of clusters. Indeed, methanol has smaller cyclic clusters involving an increase in the range of the interactions.

Additionally, in three pure TBA, ETOH, and MeOH liquids, the HOP was found equal to 14.9, 7.1, and 15.0, i.e., below 15.74, involving an absence of heterogeneity. In the *pure liquids*, this result indicates that the presence of clusters could be uncorrelated from the notion of heterogeneity, which is in line with the conclusion drawn by Perera *et al.* [33]. However, this result also suggests that the prepeak will be a structural signature of the mesoscopic correlations between cyclic clusters, which is evidence of the heterogeneity of the microscopic scale.

The spatial heterogeneity of miscible liquid mixtures then would be the result of the local structural disruption of the homogenous structure in the pure liquid. Indeed, as observed in Fig. 7, by progressively increasing the toluene concentration, the initial hydrogen-bonding network corresponding to a homogenous structure is then locally broken due to the favorable toluene-methanol interactions leading to the spatial heterogeneity. As the toluene concentration increases, the heterogeneity increases to reach a maximum around $x_{\mathrm{MeOH}} = 0.5$ (see Fig. 3). From $x_{\mathrm{MeOH}} = 0.5$ to $x_{\mathrm{MeOH}} = 0.0$ the HOP decreases, highlighting a loss of heterogeneity because the local disruption is then spatially propagated to recover an apparently homogenous structure. As shown in Figs. 2 and in 3 the nonideality of the toluene-methanol mixture is quasicorrelated to the HOP evolution and then to its structural heterogeneity.

IV. CONCLUDING REMARKS

This work has focused on the exploration at the nanoscale of the nonideality of methanol-toluene and methanol-cyclohexane binary liquid mixtures by means of molecular dynamics simulations. Simulations fairly reproduced the full miscibility of toluene in methanol, and the range of miscibility of cyclohexane was quantitatively established. In both mixtures, the deviation from the ideal mixture behavior was observed.

In the case of toluene this nonideality (positive excess density) and the miscibility have been ascribed with the specific interactions between toluene and methanol leading to a breaking in the hydrogen-bonding network involving clusters of different sizes and the spatial heterogeneity. The immiscibility and the nonideality (negative excess density) of the CHX-MeOH mixtures were the result of the unfavorable interactions between CHX and MeOH leading to a self-organizing of CHX molecules to form hydrophobic nanophases at the origin of the structural heterogeneity in the miscible region.

Nanophases have been characterized in terms of pockets of linear clusters such that the difference in miscibility and in heterogeneity were understood in terms of cluster size and distribution.

Moreover, we have shown that the presence of clusters had to be uncorrelated from the notion of heterogeneity. Eventually, we have highlighted that the prepeak observed in the structure factor is independent of the degree of heterogeneity but is rather connected to the presence of cyclic clusters.

[1] D. Rapaport, Mol. Phys. **50**, 1151 (1983).
[2] A. Luzar and D. Chandler, Phys. Rev. Lett. **76**, 928 (1996).
[3] F. H. Beijer, H. Kooijman, A. L. Spek, R. P. Sijbesma, and E. W. Meijer, Angew. Chem. Int. Ed. **37**, 75 (1998).
[4] J. Errington and P. Debenedetti, Nature (London) **409**, 318 (2001).
[5] J. Smith, C. Cappa, K. Wilson, B. Messer, R. Cohen, and R. Saykally, Science **306**, 851 (2004).

[6] T. Marechal, *The Hydrogen Bond and the Water Molecule: The Physics and Chemistry of Water, Aqueous and Bio-Media* (Elsevier, France, 2006).
[7] M. Chaplin, arXiv:0706.1355 [cond-mat.soft].
[8] A. Ghoufi, F. Artzner, and P. Malfreyt, J. Phys. Chem. B **120**, 793 (2016).
[9] E. Brini, C. Fennell, M. Fernandez-Serra, B. Hribar-Lee, M. Luksic, and K. Dill, Chem. Rev. **117**, 12385 (2017).
[10] A. Nilsson and L. Pettersson, Nat. Commun. **6**, 8998 (2015).
[11] A. Karmakar, P. Krishna, and R. Joarder, Phys. Lett. A **253**, 207 (1999).
[12] M. Tarek, D.-J. Tobias, and M.-L. Klein, Physica A **231**, 117 (1996).
[13] M. Tarek, D.-J. Tobias, and M.-L. Klein, J. Chem. Soc. Faraday Trans. **92**, 559 (1996).
[14] M. Aratono, T. Toyomasu, M. Villeneuve, Y. Uchizono, T. Takiue, K. Motomura, and N. Ikeda, J. Coll. Int. Sci. **191**, 146 (1997).
[15] S. Dixit, J. Crain, W. Poon, J. Finney, and A. Soper, Nature (London) **416**, 829 (2002).
[16] E. Stewart, R. L. Shields, and R. S. Taylor, J. Phys. Chem. B **107**, 2333 (2003).
[17] L. Dougan, S. P. Bates, R. Hargreaves, J. P. Fox, J. Crain, J. L. Finney, V. Réat, and A. K. Soper, J. Chem. Phys. **121**, 6456 (2004).
[18] S. Noskov, G. Lamoureux, and B. Roux, J. Phys. Chem. B **109**, 6705 (2005).
[19] C. Zhang and X. Yang, Fluid Phase Equilib. **231**, 1 (2005).
[20] Y. Andoh and K. Yasuoka, J. Phys. Chem. B **110**, 23264 (2006).
[21] A. Perera, F. Sokolíc, and L. Zoranić, Phys. Rev. E **75**, 060502(R) (2007).
[22] S. Stephenson, R. Offeman, G. Robertson, and W. Orts, Chem. Eng. Sci. **61**, 5834 (2006).
[23] I. Bakó, T. Megyes, S. Bálint, T. Grósz, and V. Chihaia, Phys. Chem. Chem. Phys. **10**, 5004 (2008).
[24] Y. Zhong and S. Patel, J. Chem. Phys. **113**, 767 (2009).
[25] A. Vrhovsek, O. Gereben, A. Jamnik, and L. Pusztai, J. Phys. Chem. B **115**, 13473 (2011).
[26] A. Ghoufi, I. Hureau, R. Lefort, and D. Morineau, J. Phys. Chem. C **115**, 17761 (2011).
[27] I. Juurinen, K. Nakahara, N. Ando, T. Nishiumi, H. Seta, N. Yoshida, T. Morinaga, M. Itou, T. Ninomiya, Y. Sakurai, E. Salonen, K. Nordlund, K. Hamalainen, and M. Hakala, Phys. Rev. Lett. **107**, 197401 (2011).
[28] O. Gereben and L. Pusztai, J. Phys. Chem. B **119**, 3070 (2015).
[29] M.-L. Tan, B. T. Miller, J. Te, J. R. Cendagorta, B. R. Brooks, and T. Ichiye, J. Chem. Phys. **142**, 064501 (2015).
[30] L. Hennous, A. A. Hamid, R. Lefort, D. Morineau, P. Malfreyt, and A. Ghoufi, J. Chem. Phys. **141**, 204503 (2014).
[31] I. Svishchev and P. Kusalik, J. Chem. Phys. **100**, 5165 (1994).
[32] A. Perera, Pure Appl. Chem. **88**, 189 (2016).
[33] Požar, Lovrinčević, Zoranić, Primorać, Sokolić, and F. A. Perera, Phys. Chem. Chem. Phys. **18**, 23971 (2016).
[34] M. Mhanna, R. Lefort, L. Noirez, and D. Morineau, J. Mol. Liquids **218**, 198 (2016).
[35] A. Laaksonen, P. Kusalik, and I. Svishchev, J. Phys. Chem. A **101**, 5910 (1997).
[36] J. Boyne and A. Williamson, J. Chem. Eng. Data **12**, 318 (1967).
[37] J. Kim, K. Lee, and S. Kim, J. Membr. Sci. **169**, 81 (2000).
[38] N. Hilmioglu, Manage. Environ. Qual. **20**, 165 (2009).
[39] Q. Kang, J. Huybrechts, B.-V. der Bruggen, J. Baeyens, T. Tan, and R. Dewil, Sep. Pur. Technol. **136**, 144 (2014).
[40] W. Jorgensen, D. Maxwell, and J. Tirado-Rives, J. Am. Chem. Soc. **118**, 11225 (1996).
[41] T. Pascal, S.-T. Lin, and W. A. Goddard III, Phys. Chem. Chem. Phys. **13**, 169 (2011).
[42] R. A. Zubillaga, A. Labastida, B. Cruz, J. Matinez, E. Sanchez, and J. Alejandre, J. Chem. Theory Comput. **9**, 1611 (2013).
[43] I. Todorov, W. Smith, K. Trachenko, and M. Dove, J. Mater. Chem. **16**, 1911 (2006).
[44] S. Nose, J. Chem. Phys. **81**, 511 (1984).
[45] W. G. Hoover, Phys. Rev. A **31**, 1695 (1985).
[46] A. Ghoufi and P. Malfreyt, J. Chem. Phys. **136**, 024104 (2012).
[47] M. Guo and B. C. Y. Lu, J. Chem. Phys. **106**, 3688 (1997).
[48] Y. Miyano and W. Hayduk, J. Chem. Eng. Data **38**, 277 (1993).
[49] P. Nikam, B. Jagdale, A. Sawant, and M. Hasan, J. Chem. Eng. Data **45**, 559 (2000).
[50] A. Ghoufi, F. Goujon, V. Lachet, and P. Malfreyt, J. Chem. Phys. **128**, 154716 (2008).
[51] F. Biscay, A. Ghoufi, and P. Malfreyt, J. Chem. Phys. **134**, 044709 (2011).
[52] F. Biscay, A. Ghoufi, V. Lachet, and P. Malfreyt, J. Phys. Chem. C **115**, 8670 (2011).
[53] A. Ghoufi and P. Malfreyt, Mol. Sim. **39**, 603 (2013).
[54] R. Baskaran and T. Kubendran, Russ. J. Phys. Chem. A **83**, 350 (2009).
[55] Y. Wang and G. A. Voth, J. Phys. Chem. B **110**, 18601 (2006).
[56] S. Li, J. Bañuelos, P. Zhang, G. Feng, S. Dai, G. Rother, and P. Cummings, Soft Matter **10**, 9193 (2014).
[57] D. Morineau and C. Alba-Simionesco, J. Chem. Phys. **118**, 9389 (2003).
[58] A. Ghoufi, I. Hureau, D. Morineau, R. Renou, and A. Szymczyk, J. Phys. Chem. C **117**, 15203 (2013).
[59] R. Renou, A. Szymczyk, and A. Ghoufi, J. Chem. Phys. **140**, 044704 (2014).
[60] P. Krüger, S. K. Schnell, D. Bedeaux, S. Kjelstrup, T. J. H. Vlugt, and J.-M. Simon, J. Phys. Chem. Lett. **4**, 235 (2013).
[61] N. Dawass, P. Krüger, S. K. Schnell, J.-M. Simon, and T. J. H. Vlugt, Fluid Phase Equilib. **486**, 21 (2019).